Immunotargeting of Integrin 6 4 for Single-Photon Emission Computed Tomography and Near-Infrared Fluorescence Imaging in a Pancreatic Cancer Model

Article *in* Molecular Imaging · January 2016

DOI: 10.1177/1536012115624917

8 authors, including:

Winn Aung
National Institute of Radiological Sciences
23 PUBLICATIONS **581** CITATIONS
SEE PROFILE

Hitomi Sudo
National Institute of Radiological Sciences
26 PUBLICATIONS **164** CITATIONS
SEE PROFILE

Molecular Imaging
Volume 15 : 1-11
© The Author(s) 2016
Reprints and permission:
sagepub.com/journalsPermissions.nav
DOI: 10.1177/1536012115624917
mix.sagepub.com
SAGE

Immunotargeting of Integrin $\alpha_6\beta_4$ for Single-Photon Emission Computed Tomography and Near-Infrared Fluorescence Imaging in a Pancreatic Cancer Model

Winn Aung, MBBS, PhD[1], Atsushi B. Tsuji, PhD[1], Hitomi Sudo, PhD[1], Aya Sugyo, M.Ed[1], Takako Furukawa, PhD[1], Yoshinori Ukai, PhD[2], Yoshikazu Kurosawa, PhD[3], and Tsuneo Saga, MD, PhD[1]

Abstract

To explore suitable imaging probes for early and specific detection of pancreatic cancer, we demonstrated that $\alpha_6\beta_4$ integrin is a good target and employed single-photon emission computed tomography (SPECT) or near-infrared (NIR) imaging for immunotargeting. Expression levels of $\alpha_6\beta_4$ were examined by Western blotting and flow cytometry in certain human pancreatic cancer cell lines. The human cell line BxPC-3 was used for $\alpha_6\beta_4$-positive and a mouse cell line, A4, was used for negative counterpart. We labeled antibody against $\alpha_6\beta_4$ with Indium-111 (^{111}In) or indocyanine green (ICG). After injection of ^{111}In-labeled probe to tumor-bearing mice, biodistribution, SPECT, autoradiography (ARG), and immunohistochemical (IHC) studies were conducted. After administration of ICG-labeled probe, in vivo and ex vivo NIR imaging and fluorescence microscopy of tumors were performed. BxPC-3 tumor showed a higher radioligand binding in SPECT and higher fluorescence intensity as well as a delay in the probe washout in NIR imaging when compared to A4 tumor. The biodistribution profile of ^{111}In-labeled probe, ARG, and IHC confirmed the $\alpha_6\beta_4$ specific binding of the probe. Here, we propose that $\alpha_6\beta_4$ is a desirable target for the diagnosis of pancreatic cancer and that it could be detected by radionuclide imaging and NIR imaging using a radiolabeled or ICG-labeled $\alpha_6\beta_4$ antibody.

Keywords

pancreatic cancer, integrin $\alpha_6\beta_4$, ^{111}In SPECT, NIR imaging, ICG

Introduction

Pancreatic cancer is a particularly challenging malignancy in terms of its nonspecific symptoms, delayed diagnosis, and limited therapeutic options.[1] It is a deadly disease, imposing a heavy burden to the patients. Its incidence is rising worldwide, especially in the developed countries. Unfortunately, there has been little progress in the treatment outcomes of this disease, and the mortality rates have remained the same over the past decades.[2,3] Therefore, there is an urgent need to explore suitable molecular markers and imaging probes to aid an early and specific diagnosis of pancreatic cancer.

High-throughput techniques such as gene profiling and proteomics are used to identify markers that are differentially expressed in pancreatic cancer. A family of adhesion molecules, integrins, form various heterodimer transmembrane proteins that mediate cell–cell and cell–extracellular matrix interactions.[4] They also regulate the signaling pathways essential for cancer progression, including adhesion, migration, invasion, proliferation, survival, and metastasis.[5] Among the integrins, we focused on integrin $\alpha_6\beta_4$ ($\alpha_6\beta_4$) in this study. Previously, some studies reported that $\alpha_6\beta_4$ is expressed at the

[1] Diagnostic Imaging Program, Molecular Imaging Center, National Institute of Radiological Sciences, Chiba, Japan
[2] Perseus Proteomics Inc, Tokyo, Japan
[3] Innovation Center for Advanced Medicine, Fujita Health University, Toyoake, Japan

Submitted: 15/05/2015. Revised: 27/10/2015. Accepted: 01/11/2015.

Corresponding Author:
Winn Aung, Diagnostic Imaging Program, Molecular Imaging Center, National Institute of Radiological Sciences, Anagawa 4-9-1, Inage-ku, Chiba 8555, Japan.
Email: winn@nirs.go.jp

basal surface of most epithelia and contributed to basement membranes interaction.[6] Meanwhile, $\alpha_6\beta_4$ has been identified as an antigen associated with carcinoma progression.[7] Later, increase in the expression of $\alpha_6\beta_4$ in some carcinomas in comparison to normal tissue has been observed and strengthened the association between high $\alpha_6\beta_4$ expression and cancer.[8-11] Recent gene profiling studies[12] and immunohistochemical (IHC) analyses[13,14] demonstrated that $\alpha_6\beta_4$ is overexpressed in pancreatic adenocarcinoma. Cruz-Monserrate et al reported that the majority of pancreatic adenocarcinoma samples (104 of 113, 92%) showed overexpression of $\alpha_6\beta_4$ and altered localization to the cytoplasm and membranous regions. In contrast, chronic pancreatitis samples (13 of 14, 93%) exhibited the staining pattern observed in the normal pancreas, showing localization only at the cell basal interface with the basement membrane.[13] Gleason et al also reported that β_4 integrin subunit is overexpressed in pancreatic adenocarcinoma samples (44 of 48, 92%), while chronic pancreatitis and normal pancreas specimens did not display substantial expression levels.[14] High $\alpha_6\beta_4$ expression has been detected in a variety of others tumors such as breast,[8,9,15] colon,[10] thyroid[11] cancer, and skin squamous cell carcinoma.[16]

Evidence demonstrated cooperative signaling between $\alpha_6\beta_4$ and growth factor receptors such as epidermal growth factor receptor, receptor tyrosine-protein kinase erbB-2 (ErB2), and recepteur d'origine nantais (Ron).[9,17,18] Some studies suggested that $\alpha_6\beta_4$ integrin may enhance the invasion of malignant cells by stimulating cell motility and activating intracellular signaling essential for invasion, such as the phosphatidylinositol 3-kinase (PI3K) pathway[8,19] in breast cancer. Overexpression of $\alpha_6\beta_4$, especially at the tumor-invasive front[13] and its delocalization to cell-leading edges,[20] in invasive and metastatic pancreatic carcinoma is also known. Furthermore, $\alpha_6\beta_4$ contribution to the phosphorylation of focal adhesion kinase and protein kinase B via activation of the PI3K pathway,[21] and $\alpha_6\beta_4$ requirement for the Tiam-Rac1 pathway in the migratory and invasive phenotype of pancreatic cancer[22] have been reported. Association of $\alpha_6\beta_4$ with known oncogenes such as Ras[23] and c-Met,[24] and the regulation of transcription factor nuclear factor of activated T-cells-1 (NFAT-1)[25] has also been reported, suggesting that $\alpha_6\beta_4$ cooperates to trigger oncological events and contributes to pancreatic cancer invasion and metastasis.

In addition, overexpression of $\alpha6\beta4$ is observed in early stages of pancreatic adenocarcinoma termed as pancreatic intraepithelial neoplasias (PanINs) and holds great promise as an early biomarker.[13] Taken together, $\alpha_6\beta_4$ would be a good molecular imaging target. A radiolabeled or fluorophore-labeled antibody against $\alpha_6\beta_4$ would be a promising tool for the diagnosis of pancreatic cancer. However, to the best of our knowledge, this approach has not yet been reported. We recently isolated a fully human monoclonal immunoglobulin (Ig) G_1 antibody against $\alpha_6\beta_4$, designated as ITGA6B4, from a large-scale human antibody library constructed using a phage-display system and screened using living pancreatic cancer cells.[26]

In the present study, we labeled ITGA6B4 with Indium-111 (^{111}In) for single-photon emission computed tomography (SPECT) and near-infrared (NIR) fluorophore indocyanine green (ICG) for NIR fluorescence imaging. In the clinical setting, preoperative SPECT imaging and intraoperative NIR fluorescence imaging used to delineate tumor margin could enhance the ability to diagnose, stage, and resect pancreatic cancer. Here, in vitro and in vivo properties of the probes were evaluated to assess their potential in imaging $\alpha_6\beta_4$-expressing tumors in a pancreatic cancer model.

Materials and Methods

Cell Lines

The human pancreatic cancer cell lines, namely, BxPC-3, AsPC-1, MIAPaCa-1, and PANC-1, were purchased from the American Type Culture Collection (Manassas, Virginia). A4 cells established from mouse 3T3 cells transfected with a human HER2-expression (human epidermal growth factor receptor 2) vector were used as a negative control. All cell lines were maintained and passaged in Roswell Park Memorial Institute medium (RPMI) 1640 medium (Sigma-Aldrich, St Louis, Missouri) supplemented with 10% fetal bovine serum (Nichirei Biosciences, Tokyo, Japan), 100 U/mL penicillin-G sodium, and 100 mg/mL streptomycin sulfate (Invitrogen, Carlsbad, Carlsbad) at 37°C under a humidified atmosphere containing 5% CO_2.

Animal Tumor Model

All animal experiments were carried out in accordance with the guidelines for animal experimentation determined by the Animal Care and Use Committee of our institution. A single-cell suspension of 5×10^6 BxPC-3 cells, 5×10^6 AsPC-1 cells, and 2×10^6 A4 cells in 100 μL RPMI medium was mixed with BD matrigel matrix (BD Biosciences, Bedford, Massachusetts) and subcutaneously inoculated into 3 sites (2 in the thigh and 1 in the shoulder) in nude mice (7-week-old male BALB/cA Slc-nu/nu mice, CLEA, Japan) for biodistribution study. Five million BxPC-3 cells and 2×10^6 A4 cells were inoculated in the thigh for imaging study. Both experiments were carried out 12 days after inoculation when subcutaneous tumors had attained a size of 8 to 12 mm in the longest diameter.

Western Blot Analysis

Western blotting was conducted to analyze $\alpha_6\beta_4$ expression in cultured cells. Whole cell lysates were prepared using radioimmunoprecipitation assay buffer (Wako Pure Chemical Industries, Osaka, Japan) with protease inhibitor cocktail (Sigma-Aldrich). The amount of total protein was measured using the Direct Detect spectrometer (Merck Millipore, Darmstadt, Germany). Proteins (75 mg) were separated on a 10% polyacrylamide gel (ATTO Corporation, Tokyo, Japan) and transferred to Immobilon-P membrane (Millipore, Billerica, Massachusetts). The membrane was blocked with Block-Ace reagent (Dainippon Pharmaceutical, Osaka, Japan) at room temperature (RT) for 1 hour and incubated with primary

antibodies at RT for 1 hour. Commercially available antibodies purchased from Santa Cruz Biotechnology (Santa Cruz, California), namely, rabbit anti-human β_4 integrin (H-101) polyclonal antibody, rabbit anti-human α_6 integrin (H-87) polyclonal antibody, and goat anti-human actin (C-11) antibody, were used as primary antibodies. The membrane was washed with Tris-buffered saline (TBS) and incubated with the appropriate secondary antibody, which was a horseradish peroxidase (HRP)-linked donkey antirabbit or antigoat IgG (GE Healthcare, Little Chalfont, United Kingdom; Santa Cruz Biotechnology). Immunoreactive bands were visualized using the enhanced chemiluminescence plus western blot detection system (GE Healthcare). Semiquantification was achieved by band densitometry using ImageJ 1.41o software (NIH, Bethesda, Maryland) and normalized against the actin levels for evaluation.

Fluorescent Dye Labeling of Antibody

ICG Labeling Kit-NH2 and Fluorescein Labeling Kit-NH2 were purchased from Dojindo Molecular Technologies, Inc (Rockville, Maryland). Antibody labeling was performed according to the technical manual of the labeling kit. A component of this kit, NH2-Reactive ICG or fluorescein, has a succinimidyl ester group and can easily form a covalent bond with an amino group of the antibody. In brief, NH2-reactive dyes were added to ITGA6B4 (100 μg) solution on the membrane of a filtration tube and incubated at 37°C for 10 minutes. The buffer solution was then added to the mixture and centrifuged. The conjugate was recovered by pipetting with phosphate-buffered saline (PBS). The concentration of conjugates was determined using the Direct Detect spectrometer (Merck Millipore). The absorbance of fluorescein and ICG was measured at 500 and 800 nm, respectively, with the Infinite 200 PRO multimode microplate reader (Tecan Japan Co, Ltd. Kawasaki, Japan), and the number of fluorophore molecules conjugated to each antibody was calculated. The ratio of ICG or fluorescein to antibody was 0.2 or 0.5, respectively. Antibodies were analyzed using a high-performance liquid chromatography (HPLC) system (370 PUMP and UV/VIS 157, Gilson, Middleton, Wisconsin) equipped with a Zenix SEC-300 column (Sepax Technologies, Newark, Delaware) and an isocratic mobile phase of 100 mmol/L phosphate buffer (pH 6.8) at the flow rate of 1 mL/min.

Flow Cytometric Analysis of Cellular $\alpha_6\beta_4$ Expression Levels

Cellular $\alpha_6\beta_4$ expression levels were detected using fluorescein-labeled ITGA6B4 antibody (fluorescein-ITGA6B4) as previously described.[27] The cells were incubated with the antibody for 30 minutes at 4°C in suspensions with PBS containing 1% bovine serum albumin (BSA), 1mmol/L $CaCl_2$, and 1 mmol/L $MgCl_2$. The cells were rinsed with PBS and analyzed by flow cytometry using Guava EasyCyte Plus System (Guava Technologies, Millipore, Hayward, California). Cells treated with PBS without antibody were used as negative control.

Fluorescence Microscopy Studies

BxPC-3 or A4 cells were plated on a Lab-Tek Chamber slide (Thermo Fisher Scientific, Maryland) and incubated for 18 hours. Subsequently, the culture medium was removed, and the cells were immediately stained after fixation with cold methanol for 5 minutes at −20°C. Nonspecific binding of the antibody was blocked by incubating with Block-Ace reagent (Dainippon Pharmaceutical) solution containing 10% goat serum for 30 minutes at RT. Next, the cells were incubated with the ICG-labeled ITGA6B4 (ICG-ITGA6B4) or fluorescein-ITGA6B4 diluted (1:100) in antibody diluent buffer (Dako, Glostrup, Denmark) at 4°C. After 18 hours, cells were washed with TBS, and the nuclei were stained with 4′,6-diamidino-2-phenylindole Fluoromount-G (SourthenBiotech, Birmingham, Alabama). The cells were visualized under a Keyence BZ-X700 microscope (Keyence Japan Co, Ltd, Osaka, Japan) equipped with the following filter sets: excitation wavelength 675 to 750 nm, emission wavelength 760 to 860 nm, and dichroic mirror wavelength 760 nm for ICG, and excitation wavelength 450 to 490 nm, emission wavelength 500 to 550 nm, and dichroic mirror wavelength 495 nm for fluorescein. To compare BxPC-3 and A4 cells, images were acquired using the same settings of exposure time and black balance.

Radiolabeling of Antibody

Human anti-$\alpha_6\beta_4$ monoclonal antibody (IgG_1) was labeled with ^{111}In, as reported previously.[28] In brief, the antibody solution and a chelating agent *N*-[(*R*)-2-amino-3-(*p*-isothiocyanato-phenyl)propyl]-*trans*-(*S*, *S*)-cyclohexane-1,2-diamine-*N*, *N*, *N*′, *N*″, *N*‴-pentaacetic acid (DTPA) (Macrocyclics, Dallas, Texas) were mixed in a molar ratio of 1:2.5 and incubated overnight at 37°C. The conjugation ratio of DTPA and antibody was estimated to be 1.0 to 1.6 from the ratio of ^{111}In-DTPA-antibody and ^{111}In-DTPA by isoelectric focusing. Unconjugated DTPA was removed using a Sephadex G-50 column (GE Healthcare). The obtained DTPA-conjugated antibody (10 μg in 0.1 mol/L sodium acetate buffer [pH 6.0]) was then incubated with the mixture of ^{111}In chloride (600 kBq, Nihon Medi-Physics, Tokyo, Japan) and 1 mol/L sodium acetate buffer (pH 6.0) for 30 minutes at RT. The radiolabeled antibody was purified with on a Sephadex G-50 column. The typical radiochemical purity determined by isoelectric focusing was > 99%. The radiochemical yield was approximately 80% and the specific activity was approximately 50 kBq/μg.

In Vitro Binding Assays

To examine the cell binding, cell suspensions (1.6×10^5 cells and 1.25×10^6 cells) in 1% BSA/PBS were incubated with 55 ng ^{111}In-labeled antibody via DTPA (^{111}In-DTPA-ITGA6B4) for 1 hour on ice. The cells were then washed with cold 1% BSA/PBS, collected, and the cell-bound radioactivity was counted in a gamma-counter (ALOKA, Tokyo, Japan). In

competitive inhibition assay, ^{111}In-DTPA-ITGA6B4 was incubated with 2×10^6 BxPC-3cells in the presence of varying concentrations of unlabeled antibody (0-2000 ng; intact ITGA6B4 or DTPA-conjugated ITGA6B4) for 1 hour on ice. After washing, the radioactivity bound to the cells was measured. Data analysis and estimation of dissociation constant (K_d) was performed using the GraphPad Prism software (GraphPad Software, La Jolla, California).

In Vivo *Biodistribution Study*

Tumor-bearing nude mice were intravenously injected with the ^{111}In-DTPA-ITGA6B4 (26 kBq) via the tail vein. The injected dose was adjusted to 5 μg per mouse by the addition of unlabeled ITGA6B4. At 1.5, 24, 48, 72, and 96 hours after injection, mice ($n = 5$ for each group) were euthanized, and blood was collected from the heart. The major organs and tumors were removed, weighed, and their radioactivity was measured using a gamma counter (WIZARD, PerkinElmer, Waltham, Massachusetts). Radioactivity accumulation in the tumors and tissues of interest was expressed as a percentage of the injected dose per gram of tissue normalized to a 20 g mouse body weight (% ID/g).

In Vivo SPECT/CT Imaging

For SPECT imaging, ^{111}In-DTPA-ITGA6B4 (1.85 MBq) was administered intravenously. The injected dose was adjusted to 50 μg per mouse by the addition of unlabeled ITGA6B4. At 1.5, 24, 48, 72, and 96 hours after injection, mice were anesthetized by isoflurane inhalation, and data acquisition was conducted for 10 to 25 minutes using a VECTor/CT system with clustered multipinhole high-energy collimator (MILabs, Utrecht, the Netherlands). Using PMOD positron emission tomography (PET) data analysis software (PMOD Technologies, Zurich, Switzerland), regions of interests (ROIs) were manually drawn over the tumor, and the % ID/g in the ROIs was measured for quantitative analysis. Subsequently, time activity curve of ^{111}In-DTPA-ITGA6B4 was determined. Computed tomographic image was also acquired after SPECT image acquisition, and fused images were obtained using PMOD PET data analysis software.

Postimaging Ex Vivo Autoradiography and IHC Staining

After the last imaging session of SPECT/CT at 96 hours after injection, the mouse was euthanized, and the tumors were removed and frozen. The frozen tumors were serially sectioned into 20-μm thick slices. Autoradiography (ARG) was acquired by exposing the frozen sections to an imaging plate, which was scanned with an FLA-7000 bioimaging analyzer (Fujifilms Co. Ltd, Tokyo, Japan). The serial sections were then stained for IHC examination and incubated with anti-$\alpha_6\beta_4$ antibody (ITGA6B4) or rat anti-mouse CD 31 antibody (BD Pharmingen, San Diego, California) for 1 hour at RT. HRP-labeled anti-human IgG (MBL Medical & Biological Lab, Nagoya, Japan) or HRP-linked anti-mouse IgG (BD Pharmingen) were used as secondary antibodies and incubated for 30 minutes at RT. The sections were then stained with diaminobenzidine (Dako) and the nuclei were counterstained with hematoxylin.

In Vivo NIR Fluorescence Imaging

ICG-ITGA4B6 (50 μg) was injected via the tail vein in tumor-bearing mice. The mice were anesthetized by inhalation of 2.5% isoflurane, and spectral fluorescence images were obtained using the Maestro In-Vivo Imaging System (CRi, Woburn, Massachusetts) using ICG filter sets (excitation: 700-770 nm and emission: 790 nm long pass) at various time points postinjection (1.5, 24, 48, 72, and 96 hours). The tunable filter was automatically stepped in 10-nm increments from 780 to 950 nm for ICG filter setting, while the camera sequentially captured images at each wavelength interval. The white light and the spectral fluorescence images were obtained, and the background and baseline intensities were subtracted using the Maestro software. The white light and ICG spectrum image at 820 nm were overlayed using Photoshop software (Adobe, San Jose, California). The ROIs were placed on the ICG spectrum image at 820 nm with reference to the white light image to measure the tumor fluorescence intensities (FIs). After imaging at 96 hours, the mice were euthanized, and their organs and tissues were excised and processed for ex vivo imaging. Subsequently, the tumors were frozen and sectioned for fluorescence microscopic examination, and the images were compared using the same settings of exposure time and black balance.

Statistical Analysis

Significant differences between the groups were determined by Student *t* test using Microsoft Excel software and *P* values $<.05$ were considered statistically significant.

Results

Expression in Human Pancreatic Cancer Cell Lines

Four human pancreatic cancer cell lines and murine A4 cells were examined by Western blotting for endogenous $\alpha_6\beta_4$ expression (Figure 1A). Semiquantification was achieved by normalization against actin. High β_4 and α_6 expression levels were noted in BxPC-3 and AsPC-1 cell lines, while MIAPaCa-2 and PANC-1 showed relatively low expression. In A4 cells, expression β_4 and α_6 was negligible. Our Western blot results were concordant with membranous $\alpha_6\beta_4$ expression measured by flow cytometry using the fluorescein-ITGA6B4 antibody (Figure 1B). In addition, fluorescence microscopy, after overnight incubation with fluorescein-ITGA6B4 or ICG-ITGA6B4, showed the preferential binding to the cell membrane and intracellular localization of the fluorescently labeled antibodies and confirmed the high $\alpha_6\beta_4$ expression in BxPC-3 cells but not in A4 cells (Figure 1C). To match the purpose of the study, it would be more convincing if the same human pancreatic cancer cell line with and without $\alpha_6\beta_4$ expression was used. Unfortunately, all of 4 cell lines which were available in our hand have

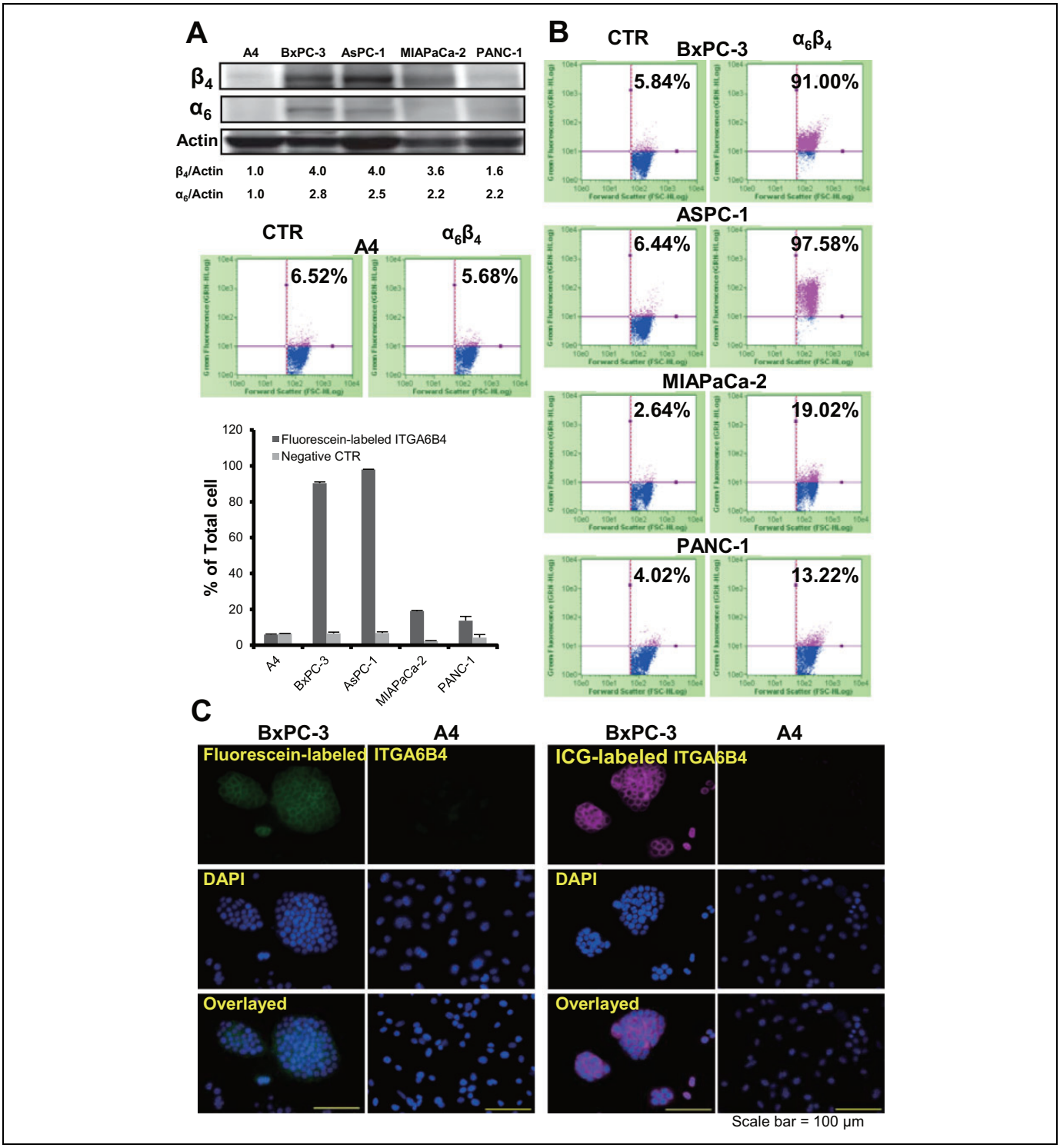

Figure 1. A, Expression of β_4 and α_6 integrins in 4 human pancreatic cancer cell lines, namely BxPC-3 (lane 2), AsPC-1 (lane 3), MIAPaCa-2 (lane 4), and PANC-1 (lane 5), were examined by Western blotting. Mouse cell line A4 (lane 1) was used as a negative control. Expression of β_4 and α_6 was normalized to actin band, and relative cell line expression standardized against to A4 cell lysate were shown under the panels. B, Expression of $\alpha_6\beta_4$ in these cell lines was compared by flow cytometric analysis. Percentages of $\alpha_6\beta_4$-positive cells (numbers in the upper-right quadrant) are presented in a bar graph. C, BxPC-3 and A4 cells were incubated with fluorescein- or ICG-labeled anti-$\alpha_6\beta_4$ antibody (ITGA6B4) for 18 hours and examined under a fluorescent microscope. Intense fluorescence signals in membrane and intracellular signals indicated the localization of each probe and confirmed the high $\alpha_6\beta_4$ expression in BxPC-3 but not in the negative control A4 cells (scale bar = 100 μm). ICG indicates indocyanine green. DAPI, 4 ,6-diamidino-2-phenylindole.

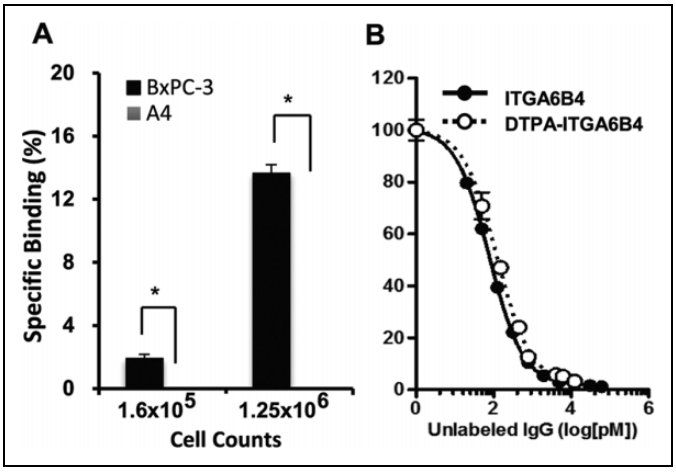

Figure 2. In vitro assay of radiolabeled anti-$\alpha_6\beta_4$ antibody (ITGA6B4) in BxPC-3 cells. A, ^{111}In-DTPA-ITGA6B4 binding increased with BxPC-3 cell concentration, however, no binding to A4 cells was observed. Data are presented as mean $\pm$ SD (n = 3 for each group; *P < .01 vs A4 cells). B, BxPC-3 cell binding was blocked by unlabeled intact ITGA6B4 (black circles) or DTPA-ITGA6B (white cycles) in the competitive inhibition assay, in a dose-dependent manner. No difference was observed in the K_d value. Data are presented as mean $\pm$ SD (n = 6 for each group). DTPA indicates *N*-[(*R*)-2-amino-3-(*p*-isothiocyanato-phenyl)propyl]-*trans*-(*S*, *S*)-cyclohexane-1,2-diamine-*N*, *N*, *N*′, *N*″, *N*″-pentaacetic acid; SD, standard deviation.

some expression, and we therefore used a murine cell line as a negative control. A human cell line for a negative control could be generated using a genome-editing method CRISPR/Cas9 system and this issue must be resolved in next study.

In Vitro Cell Binding

Cellular binding of DTPA-ITGA6B4 was evaluated in BxPC-3 and A4 cells. BxPC-3 cell binding increased with cell concentration in a dependent manner; however, no binding to A4 cells was observed (Figure 2A). In the competitive inhibition assay, the specific binding to BxPC-3 cells was blocked by the addition of unlabeled intact ITGA6B4 or DTPA-ITGA6B4 in a dose-dependent manner. The estimated K_d values were 38 pmol/L and 59 pmol/L, respectively (Figure 2B).

Biodistribution of ^{111}In-Labeled Antibody in Tumor-Bearing Mice

Radioactivity accumulation was calculated as a percentage of the injected dose per gram of tissue (% ID/g) normalized to 20 g mouse. ^{111}In-DTPA-ITGA6B4 accumulation in BxPC-3 and AsPC-1 tumors was 2.28% ID/g and 3.73% ID/g, respectively, at 1.5 hours and gradually increased with time after injection (1.5, 24, 48, 72, and 96 hours). At 96 hours, the radioactivity accumulation in BxPC-3 and AsPC-1 tumors was 46.11% ID/g and 53.76% ID/g, respectively. Meanwhile, ^{111}In-DTPA-ITGA6B4 accumulation in A4 tumor was 7.35% ID/g and 9.90% ID/g at 1.5 and 96 hours, respectively. The

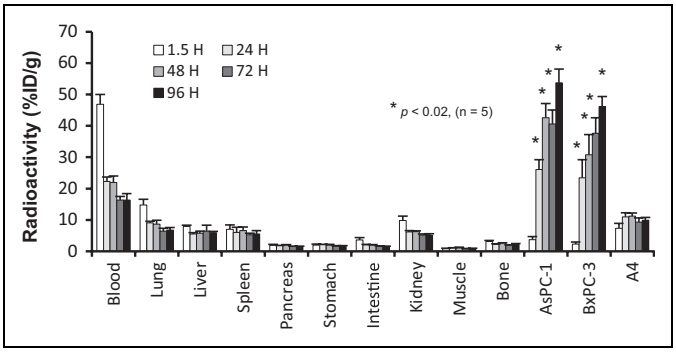

Figure 3. Biodistribution of ^{111}In-DTPA-ITGA6B4 in tumor-bearing mice. Radioactivity of samples was measured at 1.5 hours (white bar), 24 hours (pale gray bar), 48 hours (gray bar), 72 hours (dark gray bar), and 96 hours (black bar) after receiving intravenous injection of ^{111}In-DTPA-ITGA6B4. Injected dose of ^{111}In-DTPA-ITGA6B4 (26 kBq) was adjusted to 5 μg per mouse by the addition of unlabeled antibody. Data are presented as mean $\pm$ SD (n = 5 for each group; *P < .02 vs radioactivity of A4 tumor at each time point). DTPA indicates *N*-[(*R*)-2-amino-3-(*p*-isothiocyanato-phenyl)propyl]-*trans*-(*S*, *S*)-cyclohexane-1,2-diamine-*N*, *N*, *N*′, *N*″, *N*″-pentaacetic acid; SD, standard deviation

radioactivity in tissues decreased over time (Figure 3 and Supplemental table). The statistical power was 0.98, which was estimated from our tumor uptake data by calculation using G*Power software Version 3.1.9.2.[29]

In Vivo Visualization of Tumor by SPECT/CT Imaging With ^{111}In-Labeled Antibody

In parallel with the biodistribution study, we performed longitudinal SPECT imaging of the mouse bearing BxPC-3 and A4 tumors at 1.5, 24, 48, 72, and 96 hours after injection of ^{111}In-DTPA-ITGA6B4. At 1.5 hours, the radioactivity in both tumors was still low and not sufficient to observe differences, whereas blood pool radioactivity was high. Starting from 24 hours, the difference in radioactivity between tumors became evident. Markedly higher radioactivity was observed in BxPC-3 tumor compared to A4 tumor at 48, 72, and 96 hours (Figure 4A). At 48, 72, and 96 hours, BxPC-3 tumor uptakes were 28.4, 38.8, and 43.2% ID/g and A4 tumor uptakes were 10.0, 9.2, and 9.1% ID/g, respectively (Figure 4B). The probe accumulation patterns in BxPC-3 and A4 tumors were in good agreement with our biodistribution results.

Validation by Ex Vivo ARG and IHC Examination

At 96 hours, immediately after the last SPECT imaging session, the mouse was euthanized, and the tumors were removed and sectioned for ARG and IHC. On ARG images, high radioactivity was observed in BxPC-3 tumor but not in A4 tumor (Figure 4C). IHC staining of adjacent sections showed a clear difference between the tumors. BxPC-3 tumor section showed strong $\alpha_6\beta_4$ IHC staining in tumor cells, especially at the edge of the tumor–stromal interface. No $\alpha_6\beta_4$ staining was observed in A4 tumor section (Figure 4D).

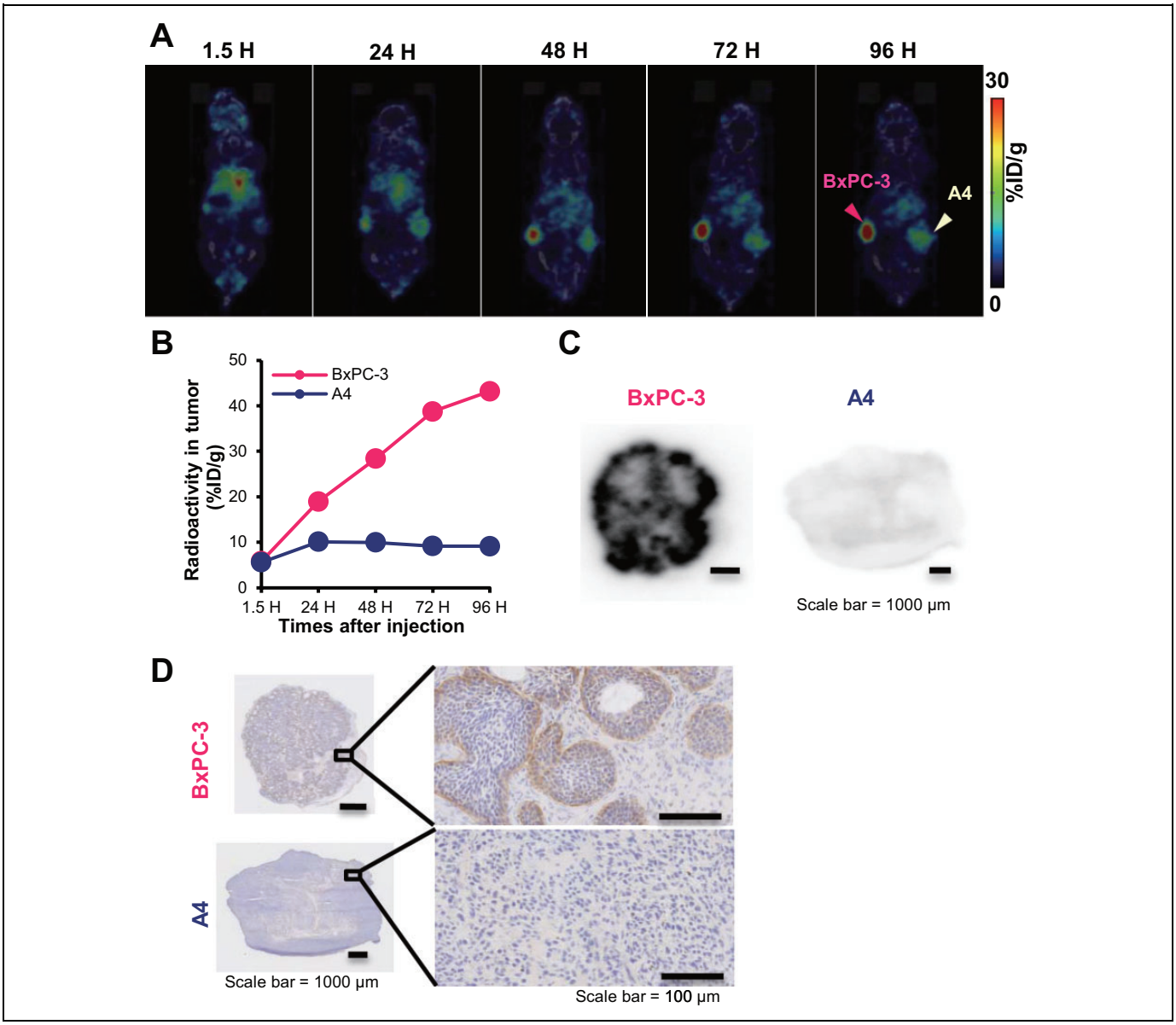

Figure 4. A, Serial SPECT/CT images of a mouse bearing xenografted target tumor (BxPC-3, pink arrowhead) and nontarget tumor (A4, white arrowhead) obtained at 1.5, 24, 48, 72, and 96 hours after injection of ^{111}In-DTPA-ITGA6B4. Injected dose of ^{111}In-DTPA-ITGA6B4 (1.85 MBq) was adjusted to 50 μg per mouse by the addition of unlabeled antibody. B, Time courses of radioactivity accumulation in both tumors were compared. C, At 96 hours, frozen BxPC-3 tumor section showed high radioactivity on ex vivo autoradiographic image, whereas A4 tumor showed no specific radioactivity (scale bar = 1000 μm). D, $\alpha_6\beta_4$ immunohistochemical staining of adjacent sections displayed strong $\alpha_6\beta_4$ staining on low- and high-power magnification in BxPC-3 tumor cells but not in A4 tumor cells (scale bar = 1000 μm at low magnification, 100 μm at high magnification). DTPA indicates *N*-[(*R*)-2-amino-3-(*p*-isothiocyanato-phenyl)propyl]-*trans*-(*S*, *S*)-cyclohexane-1,2-diamine-*N*, *N*, *N*′, *N*′′, *N*′′-pentaacetic acid; SPECT, single-photon emission computed tomography; CT, computed tomography.

In Vivo Tumor Visualization by NIR Fluorescence Imaging With ICG-Labeled Antibody

HPLC chromatograms of ICG-ITGA6B4 showed no aggregation and a monomeric form was obtained (Supplemental Figure 2). Mice bearing subcutaneous BxPC-3 and A4 tumors were intravenously injected with ICG-ITGA6B4 and imaged at the indicated time points (1.5, 24, 48, 72, and 96 hours after injection). At 1.5 hours, the fluorescence signal was visualized in the whole body, especially in abdominal region, including A4 tumor (Figure 5A). At 24 hours, the FIs of both tumors increased, and BxPC-3 tumors were more clearly visualized than A4 tumors. Moreover, the BxPC-3 tumor FI was fairly retained until 96 hours, our last time point, whereas that of A4 tumors decreased during this period (Figure 5B). In ex vivo imaging of tumors and tissues obtained from euthanized mice, BxPC-3 tumor FI was clearly identified and observed to be considerably higher than that of A4 tumors and other tissues

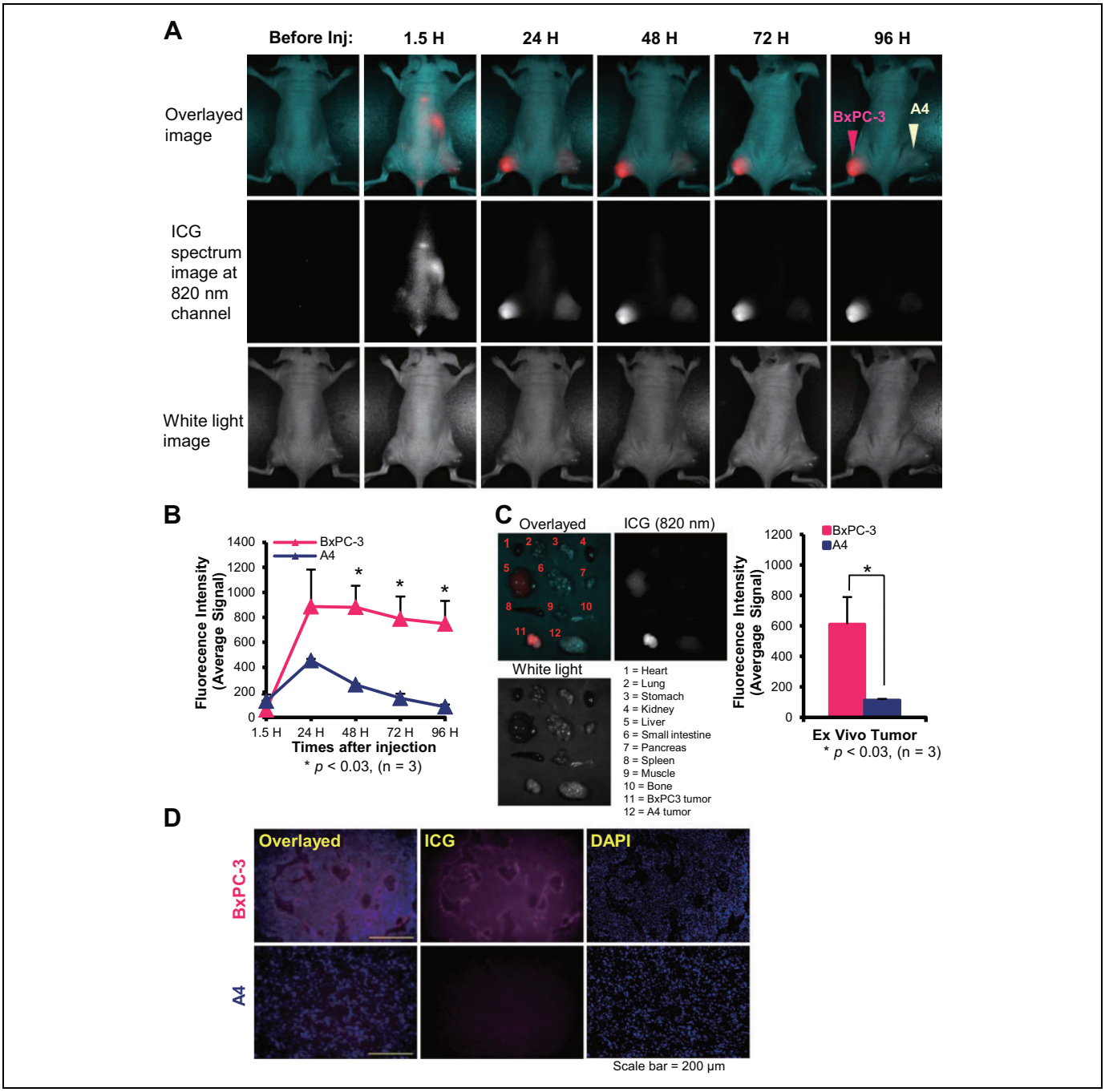

Figure 5. A, Serial NIR fluorescence imaging of a representative mouse bearing xenografted target tumor (BxPC-3, pink arrowhead) and nontarget tumor (A4, white arrowhead) was obtained before and after injection of 50 μg ICG-ITGA6B4 (1.5, 24, 48, 72, and 96 hours). The upper panel shows the overlayed image of the ICG spectrum image at 820 nm (middle panel) and the white light image (lower panel). BxPC-3 tumor FI is significantly higher than that of the A4 tumor. B, Time courses of the ICG specific FI of the 2 tumors were compared. Data are presented as mean ± SD (n = 3; *P < .03 vs FI of A4 tumor at each time point). C, Ex vivo fluorescence image of tumors and tissues obtained from euthanized mice at 96 hours after injection showed that BxPC-3 tumor emitted the highest fluorescence signal. Significantly higher FI was measured for BxPC-3 tumors. Data are presented as mean ± SD (n = 3) (*P < .03 vs FI of ex vivo A4 tumor. D, Fluorescence microscopy examination of subsequently frozen tumor section confirmed the $\alpha_6\beta_4$-specific binding of the probe in BxPC-3 tumor. Overlayed image (left panel) was obtained by fusing the ICG fluorescence image (middle panel) and DAPI nuclear staining (right panel; scale bar = 200 μm). Inj indicates injection; NIR, near-infrared; ICG, indocyanine green; SD, standard deviation; FI, fluorescence intensity; DAPI, 4′,6-diamidino-2-phenylindole.

(Figure 5C). Moreover, postimaging fluorescence microscopy of frozen sections confirmed the $\alpha_6\beta_4$ specific binding of the probe in BxPC-3 tumors (Figure 5D).

Discussion

To visualize pancreatic cancer with a targeted molecular imaging approach, a sufficient level of accessible tumor-specific targets is important to detect and delineate lesions from the background. We previously reported $\alpha_v\beta_3$ integrin and CD147 as possible targets for pancreatic cancer imaging using the $\alpha_v\beta_3$ integrin tracer ^{64}Cu-labeled cyclam-RAFT-c(-RGDfK-) peptide[27] and the ^{89}Zr-labeled anti-CD147 antibody,[30] respectively. In this study, we proposed $\alpha_6\beta_4$ as an alternative target for pancreatic cancer imaging because of its overexpresion[12-14] and roles in tumor progression. Here, we labeled a human antibody against $\alpha_6\beta_4$, designated as ITGA6B4, with the radioisotope ^{111}In or the NIR fluorophore, ICG, and examined the feasibility of these probes for pancreatic cancer imaging in an animal model.

Our Western blot analysis demonstrated a high expression of β_4 and α_6 integrin subunit in BxPC-3 and AsPC-1 pancreatic cancer cell lines and relatively low levels in MIAPaCa-2 and PANC-1 cell lines (Figure 1A). We used the commercially available anti-β_4 and α_6 integrin antibodies for Western blot analysis because our antibody, ITGA6B4, was not suitable for Western blotting. However, expression of $\alpha_6\beta_4$ in corresponding cell lysates was consistent with membranous $\alpha_6\beta_4$ expression measured by flow cytometry using fluorescein-ITGA6B4 (Figure 1B). Although it would be worthy to extend the expression analysis to a larger variety of pancreatic cancer cell lines, a limited number of cell lines were analyzed in this study, and BxPC-3 cell line was selected as the representative $\alpha_6\beta_4$-positive cell line. Fluorescence microscopy after overnight incubation with fluorescein-ITGA6B4 or ICG-ITGA6B4 confirmed the high $\alpha_6\beta_4$ expression in BxPC-3 cells and the negligible expression in A4 cells (Figure 1C).

First, we labeled ITGA6B4 with ^{111}In and evaluated its cellular binding. This probe highly and specifically bound to BxPC-3 cells but not to A4 cells (Figure 2A). In the competitive inhibition assay, the K_d of intact ITGA6B4 did not differ much from that of unlabeled DTPA-conjugated ITGA6B4, indicating that the influence of DTPA conjugation on binding affinity was minimal (Figure 2B). According to the biodistribution results, the radioactivity in BxPC-3 and AsPC-1 tumors was significantly higher than that in A4 tumors and gradually increased with time after injection (Figure 3). Antibody-mediated ^{111}In probe internalization in a previously report[28] was an encouraging characteristic to use the ^{111}In-labeled probe in antigen-targeted imaging applications. Additionally, in our study, there was a low ^{111}In-DTPA-ITGA6B4 accumulation in normal organs, including the liver, spleen, and kidney, which are the major organs for excretion of injected probe, and the pancreas. This biodistribution feature is in favor of pancreatic cancer imaging in that it produces minimal background activity. However, there may be a discrepancy between the findings obtained in mouse models and patients because ITGA6B4 antibody does not recognize murine $\alpha_6\beta_4$ integrin. It would be preferable if the detailed information about $\alpha_6\beta_4$ expression in normal human tissues and the effect of this expression on antibody localization could be added to this study. Fortunately, overexpression of $\alpha_6\beta_4$ in pancreatic adenocarcinoma samples has been reported in the literature.[13,14] In addition, the difference in expression profile of $\alpha_6\beta_4$ is expected to make $\alpha_6\beta_4$ expressed in cancer tissue more accessible to administrated antibody than $\alpha_6\beta_4$ expressed in normal tissues. So, we anticipate that further translational studies would elucidate this issue. Similar to the biodistribution results, BxPC-3 tumor showed the gradually increased accumulation of the radiolabeled probe when compared to the A4 tumor on serial SPECT (Figure 4A and B). Immediately after SPECT imaging at 96 hours after injection, BxPC-3 tumor frozen section displayed high level of radioactivity on ARG and enhanced $\alpha_6\beta_4$ IHC staining in tumor cells, especially at the edge of the tumor–stromal interface. No specific radioactivity and $\alpha_6\beta_4$ staining were observed in A4 tumor section (Figure 4C and D). Taken together, our results validated the probe-specific binding to $\alpha_6\beta_4$.

In addition to radionuclide imaging, we performed fluorescence imaging using ICG-ITGA6B4. Although ICG alone is a nonspecific probe, it has been approved by the Food and Drug Administration for clinical use since a couple of decades because of its excellent safety.[31] Moreover, the advantages of NIR properties of ICG over other visible fluorophores, such as a better tissue penetration, less autofluorescence, and large stokes shifts, allowing better rejection of excitation light,[32] convinced us to use it for antibody labeling and in vivo NIR imaging. Ogawa et al showed the feasibility of using ICG–antibody conjugates as activatable in vivo molecular imaging probes by combining ICG with directed antibody to cell-surface markers overexpressed in cancers.[33] In our study, 24 hours after injection of ICG-ITGA6B4, BxPC-3 tumor FI was considerably higher than that of A4 tumor in in vivo (Figure 5A and B) and ex vivo NIR imaging (Figure 5C), which indicated the probe-specific binding to highly expressed $\alpha_6\beta_4$. Not only the higher accumulation but also the slower washout of the probe from BxPC-3 tumors confirmed the probe specificity for $\alpha_6\beta_4$. However, it was difficult to say that nonspecific probe accumulation in tumors was totally absent because of the early rise (at 1.5 hours) and existence of fluorescence signal over the background level for some time in A4 tumors. Our IHC staining for panendothelial cell marker CD31 using anti-mouse CD31 antibody showed that A4 tumor presented a relatively rich vasculature compared to that of BxPC-3 tumor (Supplemental figure 1). Thus, we speculated that such weak fluorescence signal was most likely attributable to the diffusion of ICG-labeled molecules into the tumor because of the more permeable tumor vasculature compared to normal vessels[34] and that they were washed out rapidly due to nonbinding to the target. In light of these facts, the significantly increased accumulation of the probe in BxPC-3 tumors might be specifically associated with $\alpha_6\beta_4$ expression and specific binding of the

probe. Besides, ICG-ITGA6B4 accumulation in target (BxPC-3) and nontarget (A4) tumors on NIR imaging was almost consistent with the ^{111}In-DTPA-ITGA6B4 accumulation on SPECT imaging, except that ICG-ITGA6B4 accumulation was a little faster than that of ^{111}In-DTPA-ITGA6B4. ICG-labeled probe seemed to have slightly more rapid pharmacokinetic properties than the radiolabeled probe.

The hope for pancreatic cancer cure lies in the early detection and eradication of preinvasive lesions such as PanINs. As mentioned above, during pancreatic adenocarcinoma progression, $\alpha_6\beta_4$ is overexpressed and displays altered localization in the early stages of PanIN.[13] Thus, an earlier detection of them would increase the likelihood of a cure. The ICG-labeled probe emits the fluorescence signals in the NIR range (700-1000 nm). This is ideal for in vivo imaging because of the minimal light absorption, scattering, and autofluorescence in this range.[35] Thus, ICG-labeled probe could be used in real-time intraoperative or endoscopic/laparoscopic setting to facilitate the surgical removal of pancreatic cancer because it can delineate the tumor margin. Furthermore, ICG is one of the prospective exogenous dyes that could be used as an effective photosensitizer for photodynamic/photothermal therapy,[36] which is an advanced alternative molecular-targeted cancer therapy. Likewise, radioimmunotherapy using antibody labeled with an appropriate radionuclide (β^- and α emitter) to deliver cytotoxic radiation to a target cell is increasingly acknowledged for internal radiotherapy.[37] Thus, a radiolabeled antibody directed against $\alpha_6\beta_4$ would also be a desirable candidate. In addition, the inhibition of signaling pathways to interrupt tumor growth by $\alpha_6\beta_4$ antibody in conjunction with growth factor receptor-targeted therapies is attracting attention.[38] Altogether, $\alpha_6\beta_4$ is a good target and the molecular probes that associate to this target should be attractive and promising theranostic agents.

Conclusion

In our studies, we showed that $\alpha_6\beta_4$ status can be detected by radionuclide-based and NIR imaging techniques. In general, each technique has its own advantages as well as disadvantages, and several hurdles remained to be crossed to reach the clinical front. However, the ability to noninvasively visualize and quantify the high tumor binding of our nuclear and optical probes with specific targeting to $\alpha_6\beta_4$ in a pancreatic cancer model may offer an exceptional potential tool for diagnosis and selection of therapeutic strategies for personalized therapy in the future.

Acknowledgments

We thank all members of the Diagnostic Imaging Program, Molecular Imaging Center, NIRS, for their helpful discussions and suggestions.

Declaration of Conflicting Interests

The author(s) declared no potential conflicts of interest with respect to the research, authorship, and/or publication of this article.

Funding

The author(s) disclosed receipt of the following financial support for the research, authorship, and/or publication of this article: This study was partly supported by a Grant-in-Aid for Scientific Research (C) (24591804) from the Ministry of Education, Culture, Sports, Science and Technology, Japan. No other potential conflict of interest relevant to this article was reported.

Supplemental Material

The online [appendices/data supplements/etc] are available at http://mix.sagepub.com/supplemental

References

1. Stathis A, Moore MJ. Advanced pancreatic carcinoma: current treatment and future challenges. *Nat Rev Clin Oncol*. 2010;7(3):163-172.
2. Siegel R, Naishadham D, Jemal A. Cancer statistics, 2012. *CA Cancer J Clin*. 2012;62(1):10-29.
3. Hariharan D, Saied A, Kocher HM. Analysis of mortality rates for pancreatic cancer across the world. *HPB (Oxford)*. 2008;10(1):58-62.
4. Hynes RO. Integrins: versatility, modulation, and signaling in cell adhesion. *Cell*. 1992;69(1):11-25.
5. Desgrosellier JS, Cheresh DA. Integrins in cancer: biological implications and therapeutic opportunities. *Nature Rev Cancer*. 2010;10(1):9-22.
6. Rabinovitz I, Mercurio AM. The integrin alpha 6 beta 4 and the biology of carcinoma. *Biochem Cell Biol*. 1996;74(6):811-821.
7. Falcioni R, Sacchi A, Resau J, Kennel SJ. Monoclonal antibody to human carcinoma-associated protein complex: quantitation in normal and tumor tissue. *Cancer Res*. 1988;48(4):816-821.
8. Bon G, Folgiero V, Di Carlo S, Sacchi A, Falcioni R. Involvement of alpha(6)beta(4) integrin in the mechanisms that regulate breast cancer progression. *Breast Cancer Res*. 2007;9(1):203.
9. Soung YH, Gil HJ, Clifford JL, Chung J. Role of alpha6beta4 integrin in cell motility, invasion and metastasis of mammary tumors. *Curr Protein Pept Sci*. 2011;12(1):23-29.
10. Beaulieu JF. Integrin alpha6beta4 in colorectal cancer. *World J Gastrointest Pathophysiol*. 2010;1(1):3-11.
11. Noh TW, Soung YH, Kim HI, et al. Effect of {beta}4 integrin knockdown by RNA interference in anaplastic thyroid carcinoma. *Anticancer Res*. 2010;30(11):4485-4492.
12. Logsdon CD, Simeone DM, Binkley C, et al. Molecular profiling of pancreatic adenocarcinoma and chronic pancreatitis identifies multiple genes differentially regulated in pancreatic cancer. *Cancer Res*. 2003;63(10):2649-2657.
13. Cruz-Monserrate Z, Qiu S, Evers BM, O'Connor KL. Upregulation and redistribution of integrin alpha6beta4 expression occurs at an early stage in pancreatic adenocarcinoma progression. *Mod Pathol*. 2007;20(6):656-667.
14. Gleason B, Adley B, Rao MS, Diaz LK. Immunohistochemical detection of the beta4 integrin subunit in pancreatic adenocarcinoma. *J Histochem Cytochem*. 2005;53(6):799-801.
15. Mercurio AM, Rabinovitz I. Towards a mechanistic understanding of tumor invasion–lessons from the alpha6beta 4 integrin. *Semin Cancer Biol*. 2001;11(2):129-141.

16. Maalouf SW, Theivakumar S, Owens DM. Epidermal alpha6-beta4 integrin stimulates the influx of immunosuppressive cells during skin tumor promotion. *J Dermatol Sci*. 2012;66(2):108-118.
17. Eliceiri BP. Integrin and growth factor receptor crosstalk. *Circ Res*. 2001;89(12):1104-1110.
18. Falcioni R, Antonini A, Nistico P, et al. Alpha 6 beta 4 and alpha 6 beta 1 integrins associate with ErbB-2 in human carcinoma cell lines. *Exp Cell Res*. 1997;236(1):76-85.
19. Mercurio AM, Rabinovitz I, Shaw LM. The alpha 6 beta 4 integrin and epithelial cell migration. *Curr Opin Cell Biol*. 2001;13(5):541-545.
20. Laval S, Laklai H, Fanjul M, et al. Dual roles of hemidesmosomal proteins in the pancreatic epithelium: the phosphoinositide 3-kinase decides. *Oncogene*. 2014;33(15):1934-1944.
21. Baril P, Gangeswaran R, Mahon PC, et al. Periostin promotes invasiveness and resistance of pancreatic cancer cells to hypoxia-induced cell death: role of the beta4 integrin and the PI3 k pathway. *Oncogene*. 2007;26(14):2082-2094.
22. Cruz-Monserrate Z, O'Connor KL. Integrin alpha 6 beta 4 promotes migration, invasion through Tiam1 upregulation, and subsequent Rac activation. *Neoplasia*. 2008;10(5):408-417.
23. Dajee M, Lazarov M, Zhang JY, et al. NF-kappaB blockade and oncogenic Ras trigger invasive human epidermal neoplasia. *Nature*. 2003;421(6923):639-643.
24. Chung J, Yoon SO, Lipscomb EA, Mercurio AM. The Met receptor and alpha 6 beta 4 integrin can function independently to promote carcinoma invasion. *J Biol Chem*. 2004;279(31):32287-32293.
25. Jauliac S, López-Rodriguez C, Shaw LM, Brown LF, Rao A, Toker A. The role of NFAT transcription factors in integrin-mediated carcinoma invasion. *Nat Cell Biol*. 2002;4(7):540-544.
26. Kurosawa G, Akahori Y, Morita M, et al. Comprehensive screening for antigens overexpressed on carcinomas via isolation of human mAbs that may be therapeutic. *Proc Natl Acad Sci U S A*. 2008;105(20):7287-7292.
27. Aung W, Jin ZH, Furukawa T, et al. Micro-positron emission tomography/contrast-enhanced computed tomography imaging of orthotopic pancreatic tumor-bearing mice using the alphav-beta(3) integrin tracer (6)(4)Cu-labeled cyclam-RAFT-c (-RGDfK-)(4). *Mol Imaging*. 2013;12(6):376-387.
28. Sogawa C, Tsuji AB, Sudo H, et al. C-kit-targeted imaging of gastrointestinal stromal tumor using radiolabeled anti-c-kit monoclonal antibody in a mouse tumor model. *Nucl Med Biol*. 2010;37(2):179-187.
29. Faul F, Erdfelder E, Lang AG, et al. G*Power 3: a flexible statistical power analysis program for the social, behavioral, and biomedical sciences. *Behav Res Methods*. 2007;39:175-191.
30. Sugyo A, Tsuji AB, Sudo H, et al. Evaluation of (89)Zr-labeled human anti-CD147 monoclonal antibody as a positron emission tomography probe in a mouse model of pancreatic cancer. *Plos One*. 2013;8(4):e61230.
31. Dzurinko VL, Gurwood AS, Price JR. Intravenous and indocyanine green angiography. *Optometry*. 2004;75(12):743-755.
32. Sharma R, Wendt JA, Rasmussen JC, Adams KE, Marshall MV, Sevick-Muraca EM. New horizons for imaging lymphatic function. *Ann N Y Acad Sci*. 2008;1131:13-36.
33. Ogawa M, Kosaka N, Choyke PL, Kobayashi H. In vivo molecular imaging of cancer with a quenching near-infrared fluorescent probe using conjugates of monoclonal antibodies and indocyanine green. *Cancer Res*. 2009;69(4):1268-1272.
34. Maeda H, Matsumura Y. Tumoritropic and lymphotropic principles of macromolecular drugs. *Crit Rev Ther Drug Carrier Syst*. 1989;6(3):193-210.
35. Frangioni JV. In vivo near-infrared fluorescence imaging. *Curr Opin Chem Biol*. 2003;7(5):626-634.
36. Alander JT, Kaartinen I, Laakso A, et al. A review of indocyanine green fluorescent imaging in surgery. *Int J Biomed Imaging*. 2012;2012:940585.
37. Jain M, Gupta S, Kaur S, Ponnusamy MP, Batra SK. Emerging trends for radioimmunotherapy in solid tumors. *Cancer Biother Radiopharm*. 2013;28(9):639-650.
38. Gabarra V, Cho S, Ramirez M, et al. Antibodies directed to alpha6beta4 highlight the adhesive and signaling functions of the integrin in breast cancer cell lines. *Cancer Biol Ther*. 2010;9(6):437-445.